Electronic Supplementary Material (ESI) for Energy & Environmental Science.
This journal is © The Royal Society of Chemistry 2024

I. Supporting Text

1. Experimental Section

1.1. Chemicals

Ultra-thin and thick lithium metal foils (Kelude), Lithium Hexafluorophosphate ($LiPF_6$, DodoChem), lithium bis(fluorosulfonyl)imide (LiFSI, DodoChem), fluoroethylene carbonate (FEC, DodoChem), ethyl methyl carbonate (EMC, Adamas), 1,2-dimethoxyethane (DME, Adamas), lithium nitrate ($LiNO_3$, 99%, Macklin), ethylene carbonate (EC, Adamas), diethyl carbonate (DEC, Adamas), polyvinylidene difluoride (PVDF, DodoChem), N-methyl-2pyrrolidone (NMP, Adamas), $LiNi_{0.6}Co_{0.2}Mn_{0.2}O_2$ (NCM622, Kelude), N,N-Dimethylformamide (DMF, Adamas) are obtained as received.

1.2. Preparation of $LiNi_{0.6}Co_{0.2}Mn_{0.2}O_2$ cathode

The cathode was prepared by mixing NCM622, conductive carbon and PVDF binder with a mass ratio of 95:3:2 in NMP. The mixtures were milled by a mortar for 60 min. Slurries of cathode were coated on Al foils, then dried for 12 h under vacuum at 80℃. The normal mass loadings of the cathode were approximately 4.5 mAh cm^{-2}, and the thin NCM622 cathode is prepared with the same method with an areal capacity loading of 1.5 mAh cm^{-2}.

1.3. Preparation of electrolytes

All reagents and lithium salts are used as received without purification. 1.0 M $LiPF_6$ is dissolved in the mixture of EC/DEC with a volume ratio of 1:1 to mimic the commercial electrolyte. 1.0 M LiFSI is dissolved in the mixture of DME/FEC/EMC

with a volume ratio of 1:1:8 to obtain the W-coord electrolyte. For W&S-coord electrolyte, 3.3 M $LiNO_3$ is incorporated into DME, and this mixture is added in W-coord electrolyte. The final volume ratio of DME/FEC/EMC is 0.9:1:8. All these electrolytes are obtained under an argon-filled glove box (O_2 < 0.1 ppm and H_2O < 0.1 ppm). All the electrochemical performance shown in Figure 5 are acquired in Li||NCM622 full cells with the 70 μL electrolyte per cell. The area capacity of NCM622 is about 4.5 mAh cm^{-2}. The ratio of electrolyte to capacity (E/C) is 14 μL mAh^{-1}.

1.4. Electrochemical Measurements

NEWARE electrochemical testing systems are used to attain the cycle and rate performances. CHI Analytical Electrochemical Workstation is used to analyze the electrochemical performances. NCM622||Li cells are performed with cut-off voltage of 4.15 or 4.3 V (*vs.* Li/Li^+), respectively. All the cells are fabricated in the Argon-fill glovebox with H_2O and O_2< 0.1 ppm. Li||Cu cells are prepared by using Cu foils as working electrode and stopped at 10^{th} cycle to have the SEM images. 1.0 mAh cm^{-2} Li is plated on Cu foils and stripped until the cut-off voltage to 1 V. The ionic conductivity measurement is conducted by FE38-Standard meter (METTLER TOLEDO) at −20℃ in Thermostat (METTLER TOLEDO).

1.5. Characterization

^{27}Al spectra is collected by nuclear magnetic resonance (NMR) spectroscopy on a 600 MHz DirectDrive2 spectrometer. The morphologies of Li anode and Al foil are analyzed by scanning electron microscope (SEM, Gemini SEM 300) at 3 kV. The X-ray photoelectron spectroscopy (XPS) analysis is performed on Thermo Scientific K-

Alpha with Al K-ADES source (hν =1486.6 eV). All the XPS spectrums are energy-calibrated by the hydrocarbon peak at the binding energy of 284.8 eV.

1.6. Simulation details

Ab initio molecular dynamics (AIMD) simulation is carried out to study the corrosion mechanism of Al foil in W-coord and W&S-coord electrolyte, respectively. First, an amorphous cell is constructed with randomly packed Al^{3+}, FSI^{-}, NO_3^{-}, EMC, DME, and FEC with certain ratio (**Table S1, S2**). The solution structure is then optimized with the COMPASS II force field. The optimized cells are first simulated by classical MD at 298 K. Molecular dynamics (MD) simulations are performed using the Materials Studio 2020. The simulation is running at 298K. The time step is fixed to be 1 fs for all simulations. The systems are first equilibrated in an isobaric-isothermal (NPT) ensemble for 4 ns to maintain a temperature of 298 K and a pressure of 1 atm with time constants of 0.1 and 1 ps, respectively. A production run of 4 ns at 298 K in a canonical (NVT) ensemble under Nose–Hoover thermostat is finally conducted. The simulations are output every 1000 steps and used for the analysis of the radial distribution function. All the classical MD simulations are done through forcite modulus in Materials Studio 2020. The binding energy is calculated from Dmol3 module that obtained with the GGA-PBE method shown in **Figure S1**.

1.7. The detailed discussion of oxidation peak in LSV curves.

There are two possible reasons for the oxidation peak: (1) The oxidative decomposition of DME; (2) LiFSI corrodes Al foil. Many literatures have reported that ethers are unsuitable for high-voltage LIB especially matched with ternary

$Li(Ni_xCo_yMn_z)O_2$ (NCM) and spinel $LiNi_{0.5}Mn_{1.5}O_4$(LNMO) [1-3]. The O atom in ether group with two lone pairs of electrons exhibits evident nucleophilicity, meaning it can be oxidized and decomposed under the influence of electronic effect especially at high voltage [4]. Meanwhile, extensive literatures have reported that imide-based lithium salts would corrode Al foil during 3.6-4.2 V[5-8].

To confirm whether the oxidation peak at 3.6 V (**Figure 2**a) was related to Al foil corrosion or DME decomposition, a set of experiments were arranged, including: (i) 1 M LiFSI in DME, (ii) 1 M LiFSI in DEC, (iii) 1 M LiDFOB in DME, and (iv) 1 M LiDFOB in DEC (**Figure S2**). Linear sweep voltammogram (LSV) was performed with different electrolytes in Li||Al cells. The Li||Al cell with 1 M LiFSI in DME delivers a significant anodic current about 3.6 V vs. Li^+/Li, which is similar to the signal in **Figure 2**a. When the DME was substituted with DEC, the oxidation signal delay occurs at 4.0 V. However, when LiFSI is replaced by LiDFOB, the oxidation current is increased to 5.0 V. These demonstrate that the signal at 3.6 V meanly attributed to the corrosion of Al surface by LiFSI instead of DME decomposition. When the LiFSI and DME were both substituted with LiDFOB and DEC, no signals were detected throughout the testing process, which illustrate that the DEC is more stable than DME. As such, we tend to attribute the oxidation signal at 3.6 V to the corrosion of LiFSI on Al foil, instead of DME decomposition.

2. Supporting Tables

Table S1 The number of molecular in amorphous cell with NO_3^-.

Items (Add NO_3^-)	Quantities
Al^{3+}	100
FSI^-	150
NO_3^-	150
EMC	800
FEC	100
DME	100

Table S2 The number of molecular in amorphous cell without NO_3^-.

Items (Without NO_3^-)	Quantities
Al^{3+}	100
FSI^-	300
EMC	800
FEC	100
DME	100

3. Supporting Figures

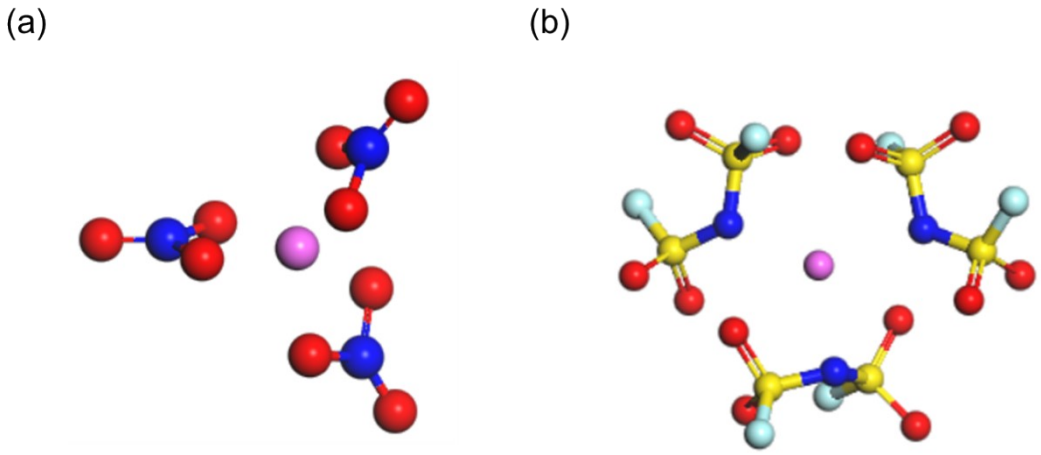

Figure S1. The optimized structures of (a) $Al(NO_3)_3$ and (b) $Al(FSI)_3$ are obtained from dmol3 module that is attained with the GGA-PBE method.

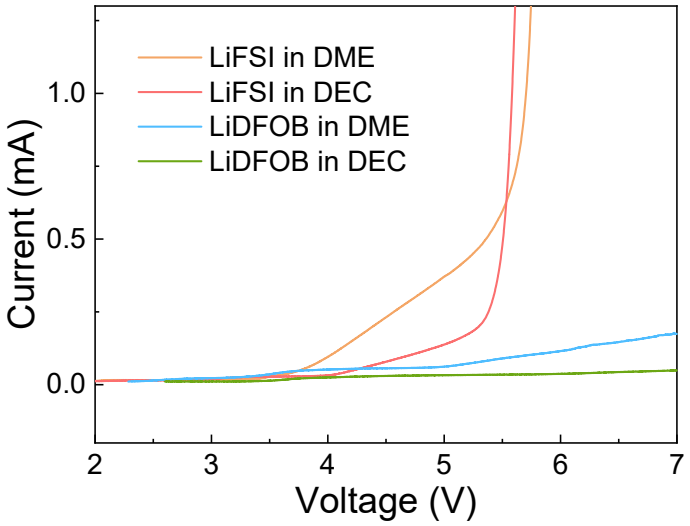

Figure S2. The oxidative stability of electrolytes measured via LSV in Li||Al cells.

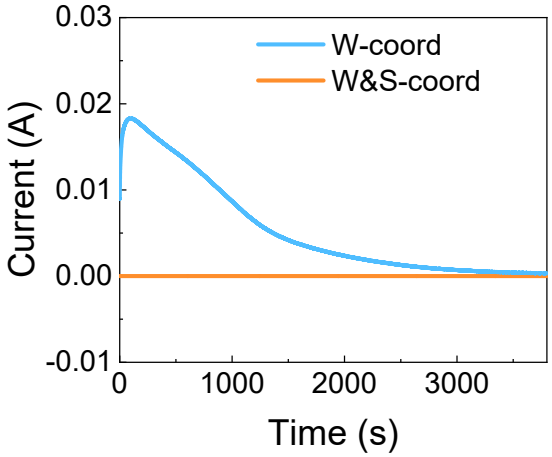

Figure S3. Typical current–time curves collected during a potentiostatic etching measurement using Al foil as working electrode. The potential is first scanned from the open circuit potential (OCP) to 4.5 V with 5 mV s^{-1}, followed by a constant potential step at 4.5 V for 4000 s.

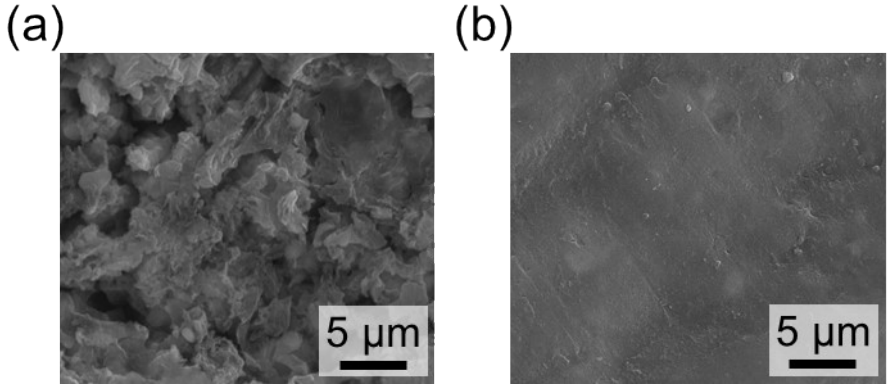

Figure S4. SEM images of Al foil etched at 4.5 V in (a) W-coord electrolyte and (b) W&S-coord electrolyte at −20℃. All the Al current collector were etched for 20 h.

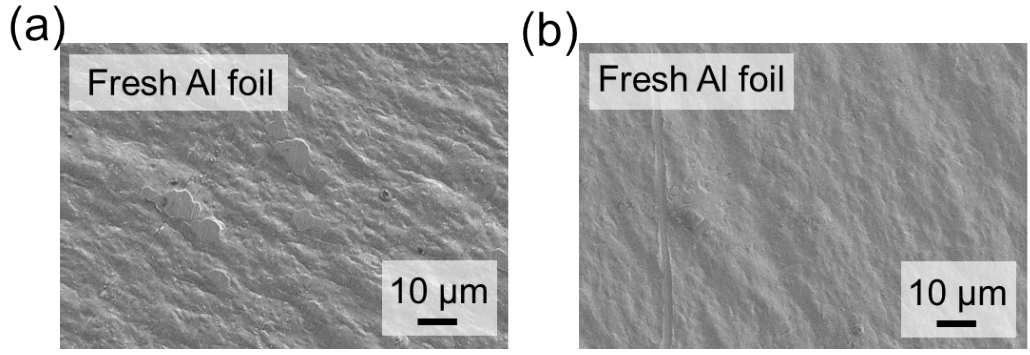

Figure S5. (a) SEM images were acquired at different positions of fresh Al foil.

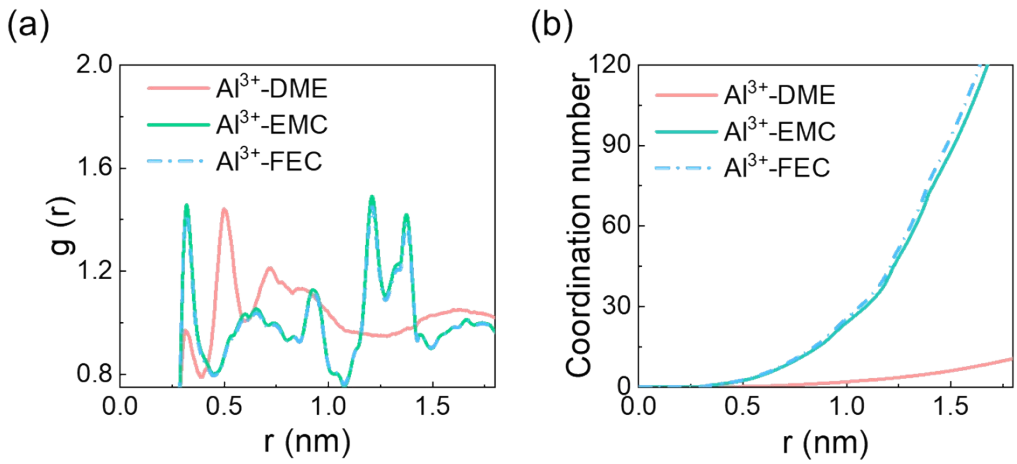

Figure S6. (a) RDF and (b) coordination number of Al^{3+}–DME, Al^{3+}–EMC and Al^{3+}–FEC in W&S-coord electrolyte simulation system.

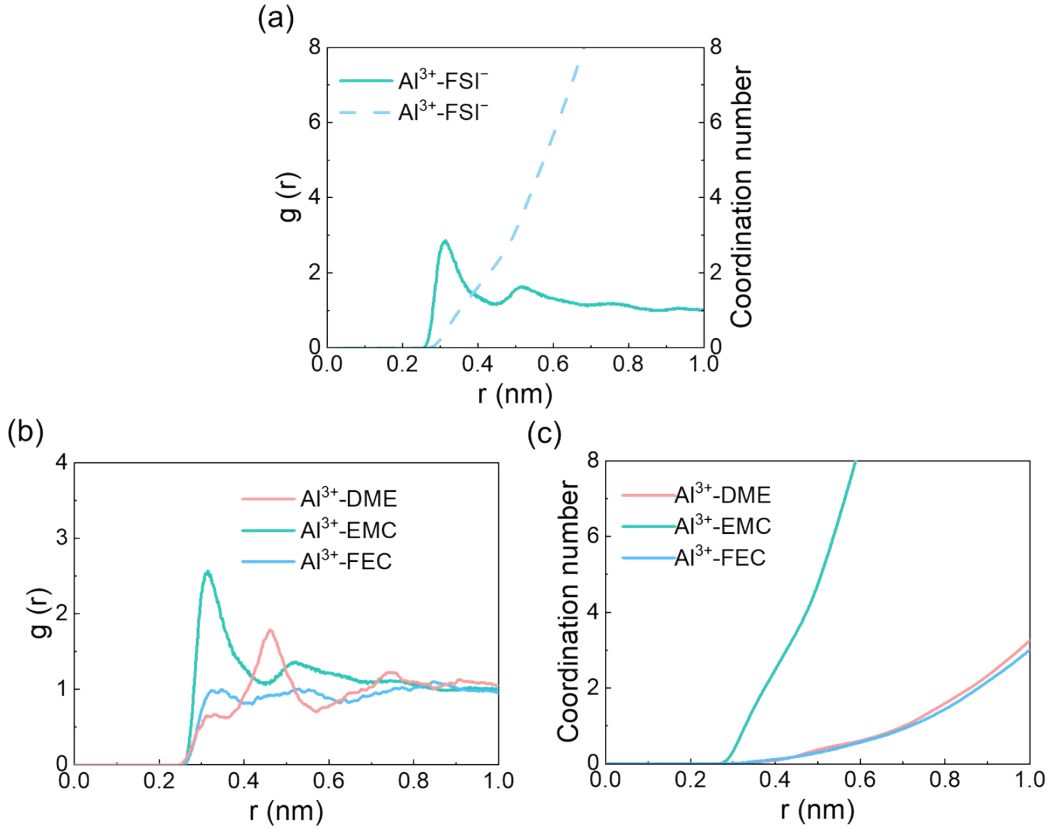

Figure S7. (a) RDF and coordination number of Al^{3+}–FSI^{-} in W-coord electrolyte simulation system. (b) RDF and (c) coordination number of Al^{3+}–DME, Al^{3+}–EMC and Al^{3+}–FEC in W-coord electrolyte simulation system.

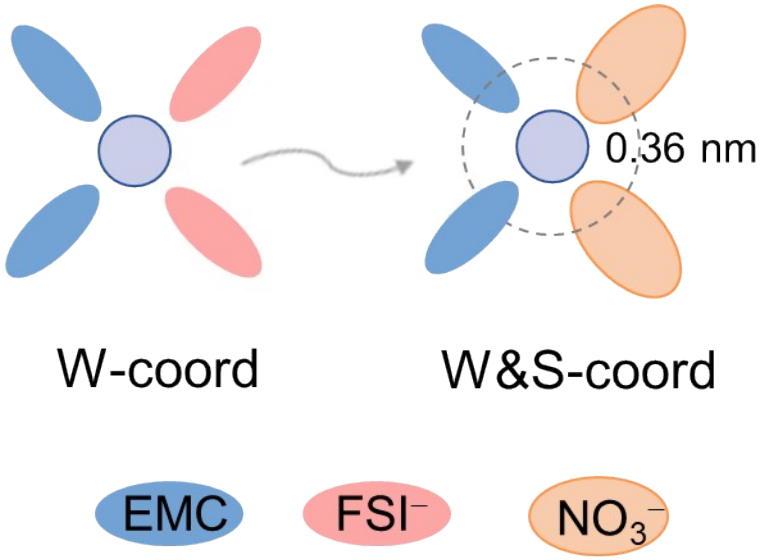

Figure S8. Possible solvation structures of Al^{3+} in W-coord and W&S-coord electrolytes.

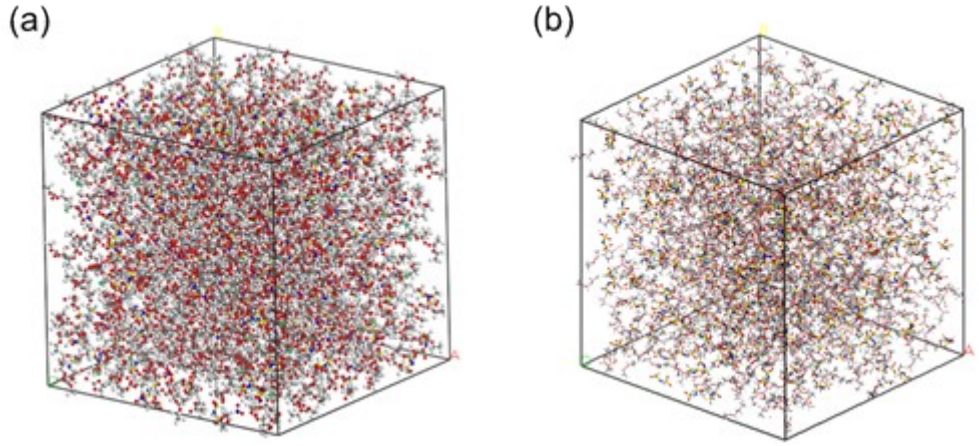

Figure S9. Snapshots of (a) W&S-coord and (b) W-coord electrolyte simulation systems given by MD simulation boxes.

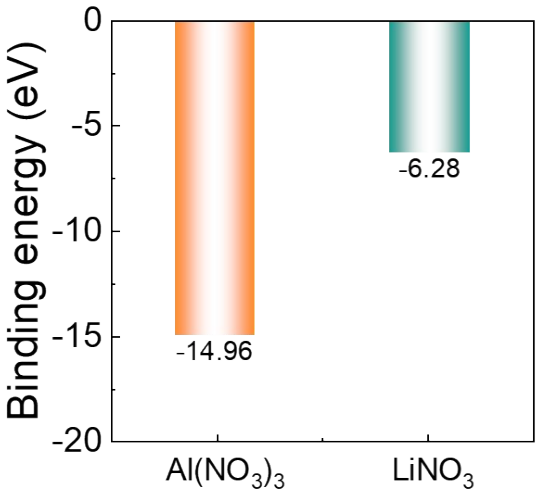

Figure S10. The binding energy of Al^{3+} and Li^{+} toward and NO_3^{-}. The calculation results are obtained with GGA-PBE method.

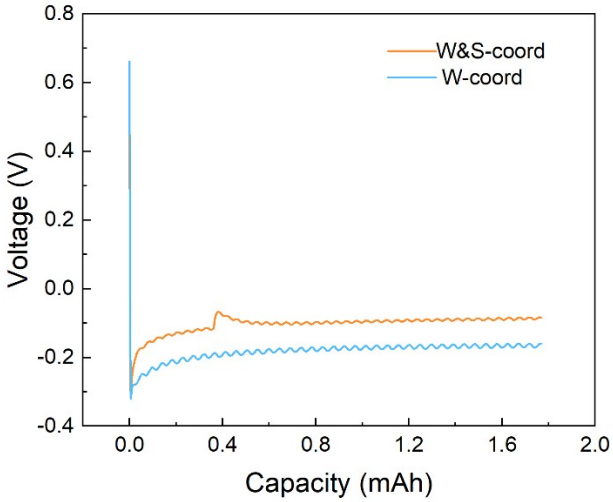

Figure S11. Primary discharge curve of the Li-Cu cell tested at 1.0 mA cm^{-2} with a plating capacity of 1 mAh cm^{-2}. (Note: the sharp rise in the voltage curve is caused by a sudden change in the temperature of the cryochamber at ~0.4 mAh.)

The experimental results show that the addition of $LiNO_3$ has a negligible effect on the very early stage of nucleation, with the overpotential of W&S-coord cell similar to the one with W-coord electrolytes at −20°C. The Li plating potential of the cell with W&S-coord electrolyte (−0.1 V) is even lower than the W-coord one (−0.18 V) in the subsequent Li propagation, indicating that $LiNO_3$ can further reduce the energy barrier of Li plating. The above results indicate that the addition of NO_3^- does not penalize the low-temperature performance.

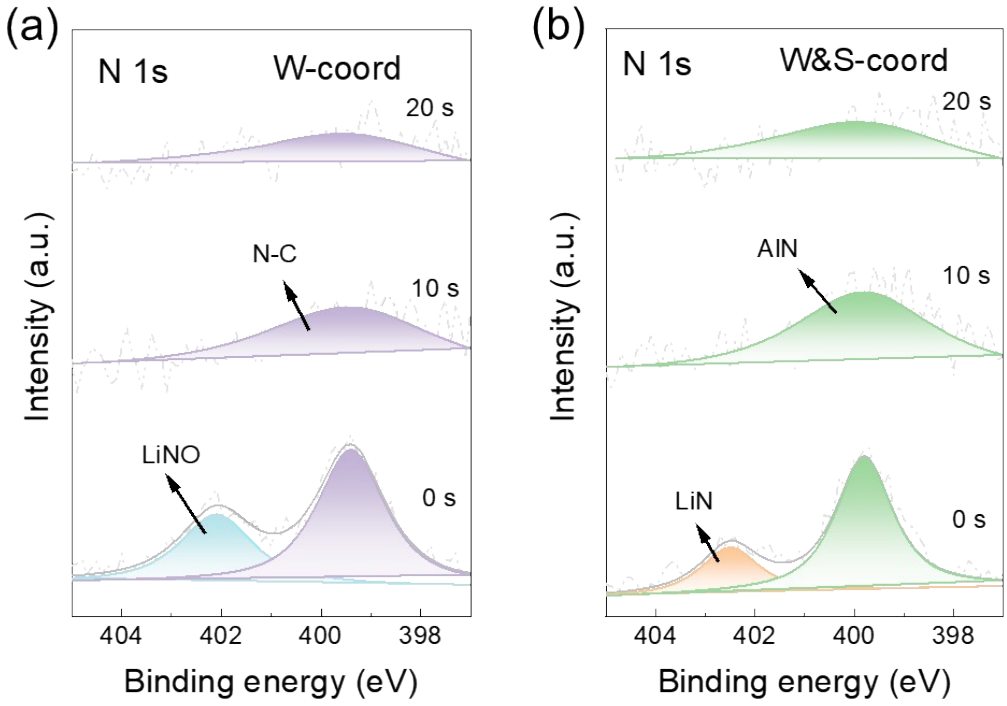

Figure S12. The N1s XPS profiles of the Al foils obtained in (a) W-coord electrolyte and (b) W&S-coord electrolyte after potentiostatic etching measurement at 4.5 V.

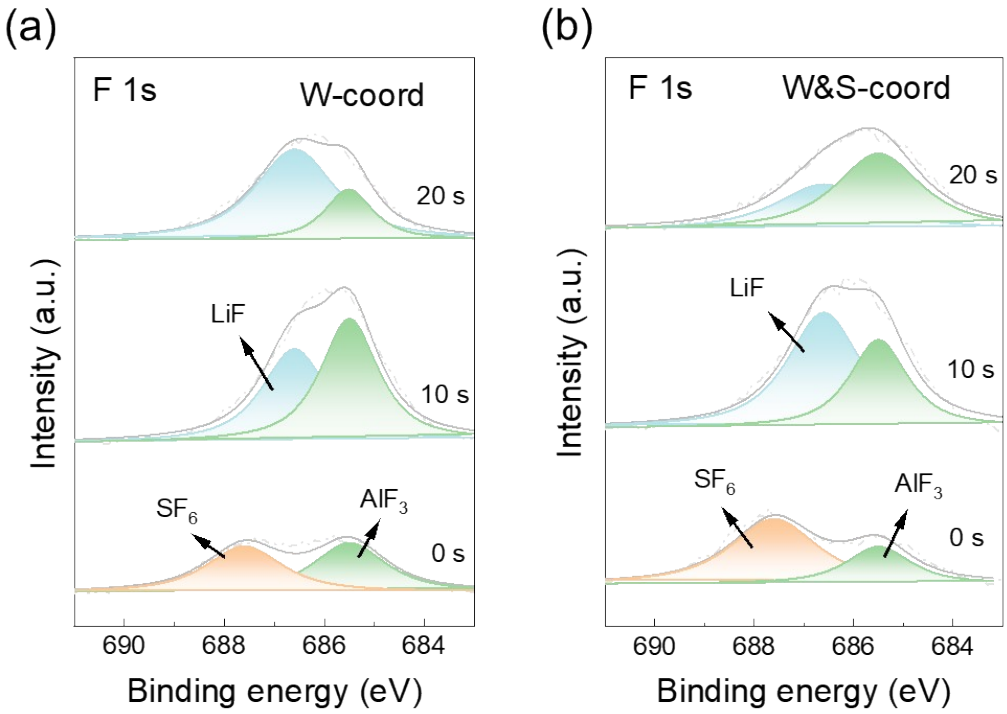

Figure S13. The F1s XPS profiles of the Al foils obtained in (a) W-coord electrolyte and (b) W&S-coord electrolyte after potentiostatic etching measurement at 4.5 V.

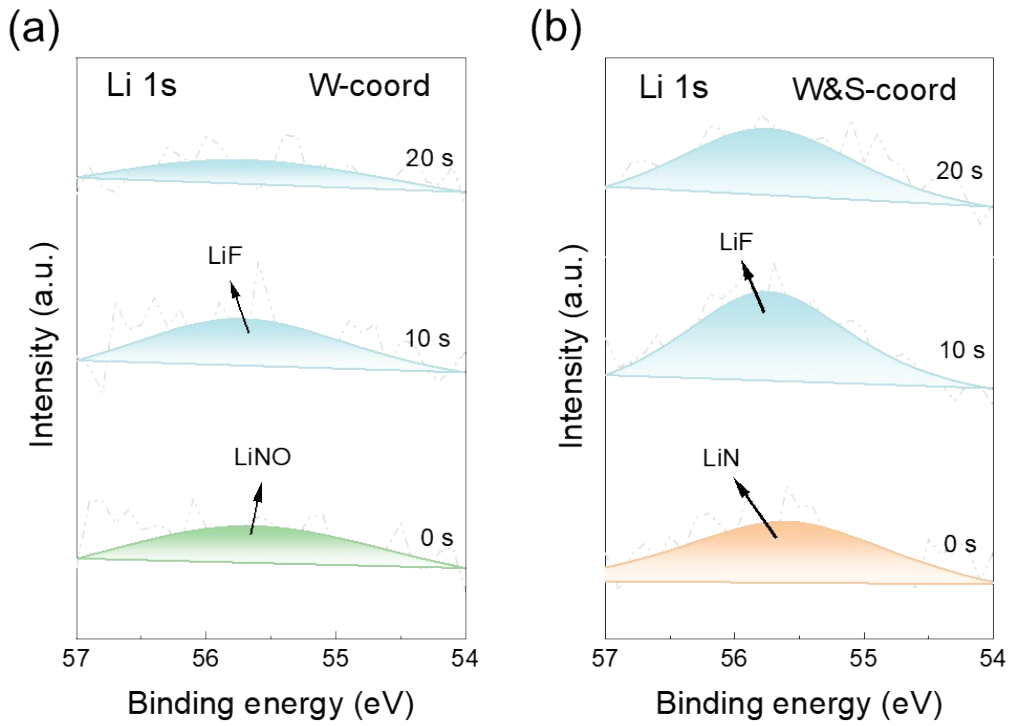

Figure S14. The Li1s XPS profiles of the Al foils obtained in (a) W-coord electrolyte and (b) W&S-coord electrolyte after potentiostatic etching measurement at 4.5 V.

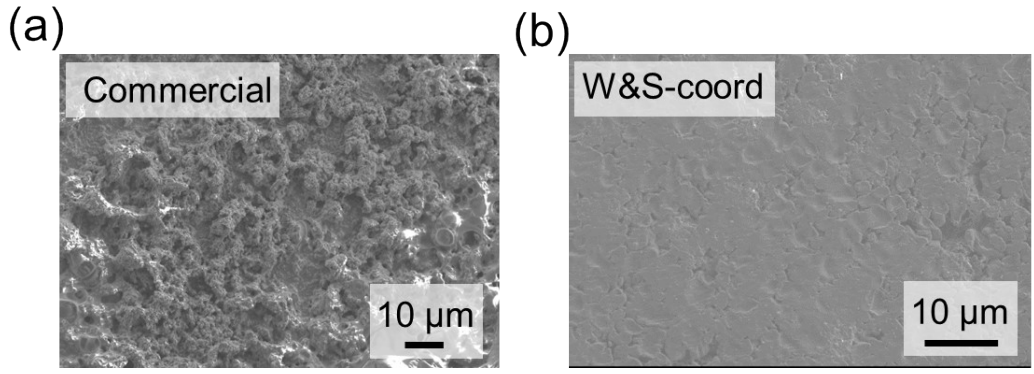

Figure S15. SEM images of Cu surface after depositing 1.0 mAh cm^{-2} Li in Li||Cu cells using (a) commercial and (b) W&S-coord electrolytes after 10 cycles.

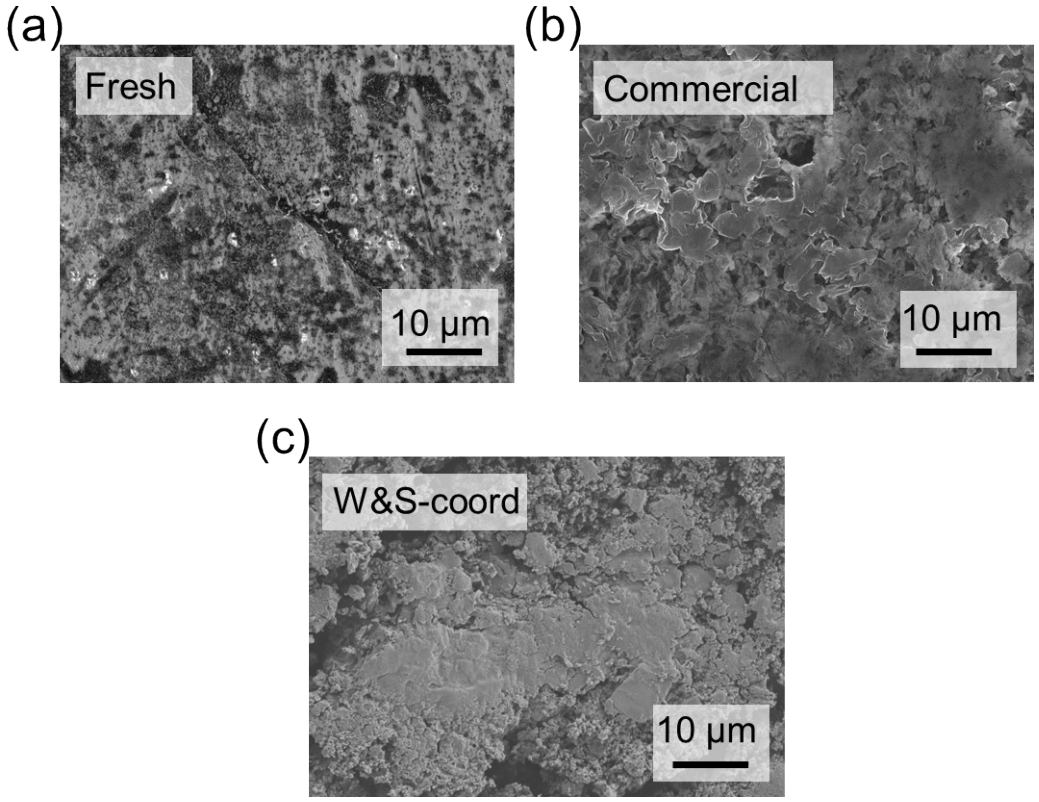

Figure S16. SEM images of Li anode surface. (a) Fresh Li foil, (b) Li anode in commercial electrolyte after 70 cycles, and (c) Li anode in W&S-coord electrolyte after 220 cycles. Cells are cycled with Li||NCM622.

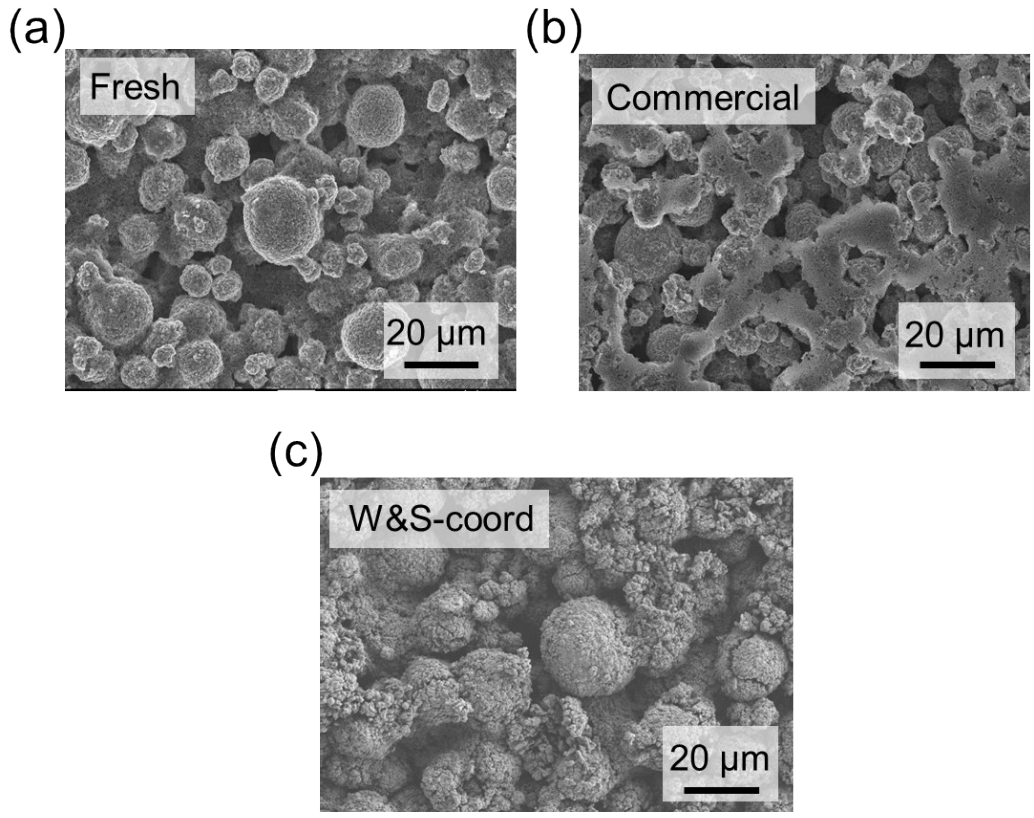

Figure S17. SEM images of NCM622 surface. (a) Fresh NCM622, (b) NCM622 in commercial electrolyte after 70 cycles, and (c) NCM622 in W&S-coord electrolyte after 220 cycles. Cells are cycled with Li||NCM622.

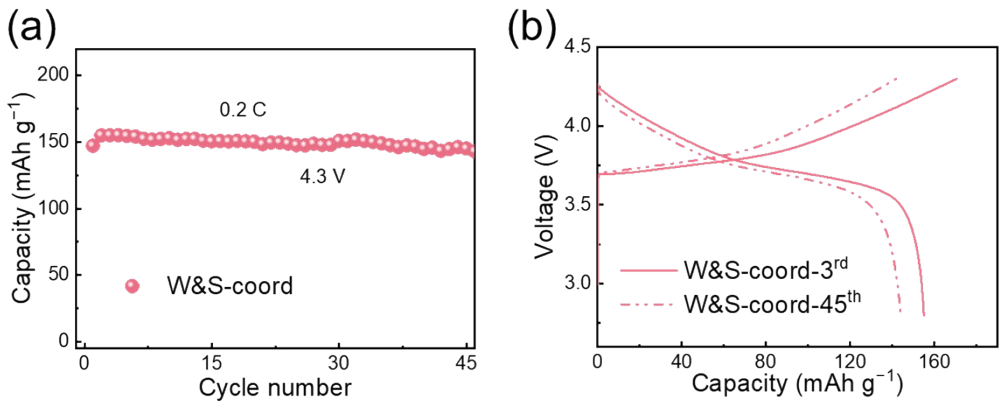

Figure S18. (a) Cycling performance of Li||NMC622 coin cells with the upper cut-off voltage of 4.3 V at 0.2 C. (b) The corresponding charge/discharge curves.

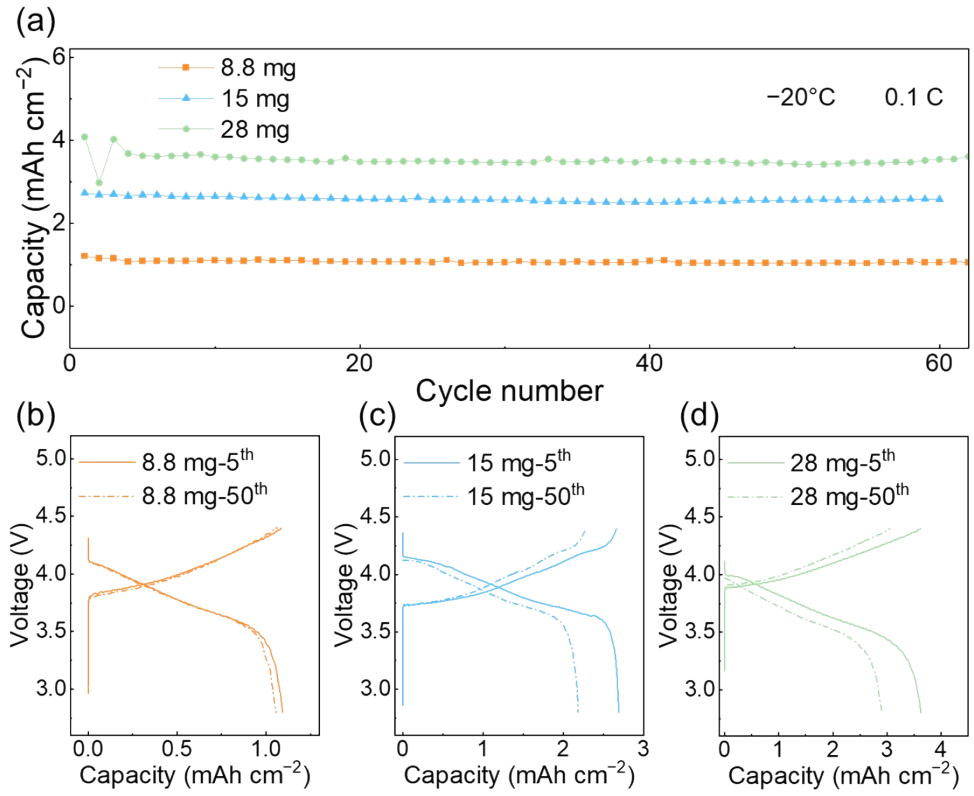

Figure S19. (a) The electrochemical performance of Li||NMC811 cells with the upper cut-off voltage of 4.4 V at 0.1 C under −20°C. (b, c, d) The corresponding charge/discharge curves of (a).

Reference

1. Y. Zhao, T. Zhou, T. Ashirov, M. E. Kazzi, C. Cancellieri, L. P. H. Jeurgens, J. W. Choi and A. Coskun, *Nat. Commun.*, 2022, **13**, 2575.
2. C. V. Amanchukwu, Z. Yu, X. Kong, J. Qin, Y. Cui and Z. Bao, *J. Am. Chem. Soc.*, 2020, **142**, 7393-7403.
3. Z. Cui, S. Chen, Q. Nian, Y. Li, Y. Chen, B.-Q. Xiong, Z. Wang, Z. He, S. Jiao and X. Ren, *J. Energy Chem.*, 2023, **79**, 110-117.
4. K. Ding, C. Xu, Z. Peng, X. Long, J. Shi, Z. Li, Y. Zhang, J. Lai, L. Chen, Y.-P. Cai and Q. Zheng, *ACS Appl. Mater. Interfaces*, 2022, **14**, 44470-44478.
5. C. L. Li, S. W. Zeng, P. Wang, Z. J. Li, L. Yang, D. N. Zhao, J. Wang, H. N. Liu and S. Y. Li, *Transactions of Nonferrous Metals Society of China*, 2021, **31**, 1439-1451.
6. L. J. Krause, W. Lamanna, J. Summerfield, M. Engle, G. Korba, R. Loch and R. Atanasoski, *J. Power Sources*, 1997, **68**, 320-325.
7. A. Abouimrane, J. Ding and I. J. Davidson, *J. Power Sources*, 2009, **189**, 693-696.
8. H. Wu, Z. Song, X. Wang, W. Feng, Z. Zhou and H. Zhang, *Nano Res.*, 2022, **16**, 8269-8280.